Journal of ELECTRONIC MATERIALS, Vol. 44, No. 10, 2015
DOI: 10.1007/s11664-015-3730-8

Structure, Ferroelectric and Photoluminescence Properties of Eu-Doped $CaBi_4Ti_4O_{15}$ Multifunctional Ceramics

XIAOCHUN WU,[1,2] PING XIAO,[1] YONGQUAN GUO,[1] QIAOJI ZHENG,[1] and DUNMIN LIN[1]

1.—College of Chemistry and Materials Science, Sichuan Normal University, Chengdu 610066, China. 2.—e-mail: wuxiaochun@sicnu.edu.cn

Lead-free multifunctional ceramics of $CaBi_{4-x}Eu_xTi_4O_{15}$ were prepared by a traditional solid state method, and the effects of Eu doping on structure, ferroelectric, piezoelectric and photoluminescence properties of the ceramics were investigated. All the ceramics possessed typical bismuth layer structure with $m = 4$, belonging to orthorhombic symmetry, and no secondary phase was detected. The plate-like grains were observed in all the ceramics, and the grain growth was slightly inhibited after the addition of Eu. Saturated polarization hysteresis loops were observed for all the ceramics, and the remanent polarization P_r decreased with Eu doping. The Eu-doped ceramics had a sharp excitation band centered at 465 nm due to the f–f transition from the $^7F_0$ ground state to the $^5D_2$ excited state of Eu^{3+}. Under the excitation by 465 nm light, the main emission peaks located at 595 nm and 616 nm were obtained, which corresponds to the transition of $^5D_0$–$^7F_1$, $5D_0$–$^7F_2$ levels in Eu^{3+}, respectively. Our study shows that $CaBi_4Ti_4O_{15}$ ceramics may be a promising multifunctional material for potential applications in optical-electro integration devices.

Key words: Aurivillius-type ceramics, ferroelectric properties, photoluminescence, $CaBi_4Ti_4O_{15}$

INTRODUCTION

$Pb(Fe_{1/2}Nb_{1/2})O_3$-$PbTiO_3$ and $Pb(Mg_{1/3}Nb_{2/3})O_3$-$PbTiO_3$ ferroelectric materials have been widely used in actuators, sensors and transducers due to their superior electrical properties.[1,2] However, the use of these ceramics led to serious environmental pollution problems. In addition, these perovskite lead-based ceramics generally possess a relatively low Curie temperature (~300–400°C) and thus are not suitable for high-temperature applications. Therefore, the investigation of lead-free materials with a high Curie temperature has attracted much attention in recent years.

Bismuth oxide layer-structured ferroelectrics (BLSFs) have been extensively studied due to their high Curie temperature. The general formula of these materials can be expressed as $(Bi_2O_2)^{2+}[A_{m-1}B_mO_{3m+1}]$,[2,3] where A is the mono-, di-, or trivalent ions or a mixture of them with coordination number 12 (e.g., K^+, Ca^{2+}, Pb^{2+}, Bi^{3+}, La^{3+}, etc.), B denotes the tetra-, penta-, or hexavalent ions or a mixture of them with coordination number 6 (e.g., Fe^{3+}, Cr^{3+}, Ti^{4+}, Ta^{5+}, W^{6+}, etc.), and m and $m - 1$ represent the numbers of oxygen octahedron and pseudo-perovskite units in the pseudo-perovskite layers interleaving with $(Bi_2O_2)^{2+}$ layers along the c-axis, respectively. As the $m = 4$ member of the BLSFs materials, $CaBi_4Ti_4O_{15}$ (CBT) with the high Curie temperature of 790°C was extensively studied and considered as a promising candidate for high-temperature applications. Many studies have been carried out to improve the electrical properties of the CBT ceramics, such as the substitution of analogous ions for A-sites ions and/or B-sites ions.[4–7] Among these studies, the substitution of rare earth ions has attracted much attention because the

(Received October 11, 2014; accepted March 5, 2015; published online April 23, 2015)

doping of BLSFs by rare earth ions not only improves the electrical properties but can also be used as luminous centers to design a large number of luminescence materials.[8–11] It can be noted that Eu has been introduced into many host phosphors materials to induce luminescence properties (e.g., $Sr_4Al_{14}O_{25}$, $Ba_3Y(PO_4)_3$, $CoFe_2O_4$@YVO_4, etc.).[12–14] Recently, several multifunctional BLSFs materials with doping by rare earth ions have been studied, and these ceramics possess simultaneously ferroelectric, piezoelectric and photoluminescence properties (e.g., Pr-doped $CaBi_2Nb_2O_9$, Ho-doped $Bi_4Ti_3O_{12}$ and Eu-doped $SrBi_2Ta_2O_9$, etc.).[15–17] However, to our knowledge, there are few reports on Eu-doped CBT and its multifunctional properties. In this work, $CaBi_{4-x}Eu_xTi_4O_{15}$ (CBT-Eu-x) ceramics with pure bismuth oxide-layered structure were successfully synthesized by a traditional solid state method, and their structure, ferroelectric and photoluminescence properties were investigated.

EXPERIMENTAL

The $CaBi_{4-x}Eu_xTi_4O_{15}$ (CBT-Eu-x) ceramics were fabricated by a traditional solid state reaction method. Raw materials were Bi_2O_3 (99.0%; Xilong chemical, China), $CaCO_3$ (99.85%; Zhongxing Electronic, China), TiO_2 (99.88%; Zhongxing Electronic, China) and Eu_2O_3 (99.99%; Sinopharm, China). All raw materials in the stoichiometric ratio of CBT-Eu-x were mixed thoroughly in ethanol using zirconia balls for 8 h, then dried and calcined at 850°C for 4 h in an alumina crucible. After calcination, the mixtures were ball-milled again. The powders were mixed with a PVA binder solution, then pressed to disk samples and finally sintered at 1180°C for 2 h in the air. Silver electrodes were fired on the top and bottom surfaces of the samples at 650°C for 30 min. The samples were poled at 180°C in a silicone oil bath for 20 min and then cooled to room temperature under a dc field of 8 kV/mm.

The crystalline structure of the sintered samples was examined using x-ray diffraction (XRD) analysis with Cu$K\alpha$ (λ = 1.540598 Å) radiation (Smart Lab; Rigaku, Tokyo, Japan), 0.01° scan step and

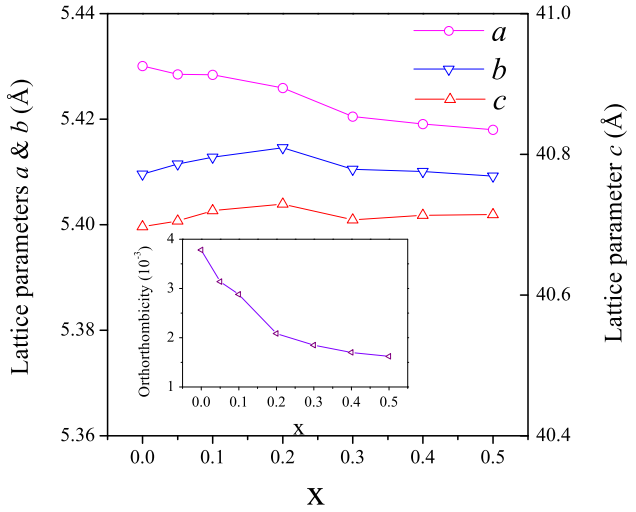

Fig. 2. Lattice parameters a, b and c as a function of x in CBT-Eu-x ceramics.

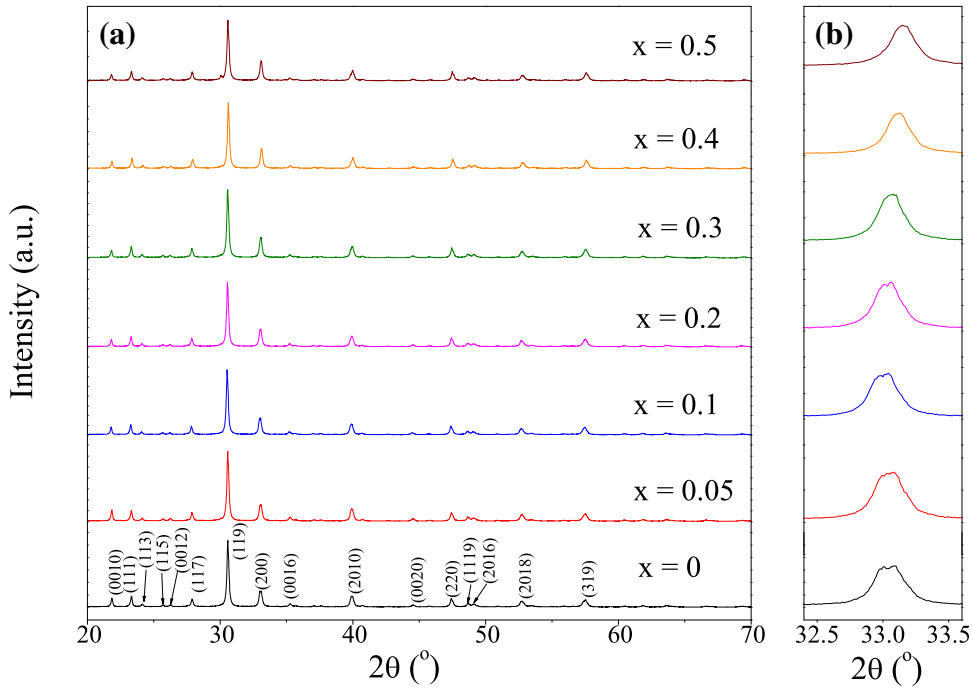

Fig. 1. The XRD patterns of the CBT-Eu-x ceramics with (a) 2θ = 20°–70° and (b) 2θ = 32°–34°.

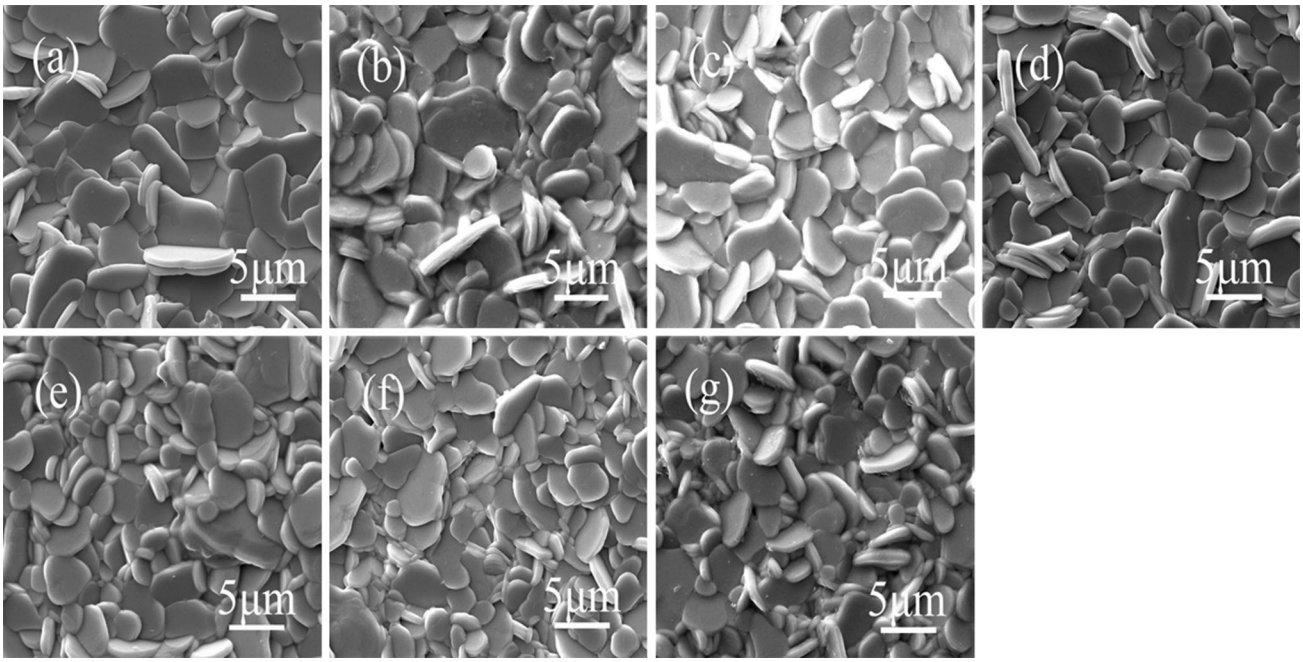

Fig. 3. SEM patterns recorded from CBT-Eu-*x* ceramics with *x* = 0 (a), 0.05 (b), 0.1 (c), 0.2 (d), 0.3 (e), 0.4 (f) and 0.5 (g).

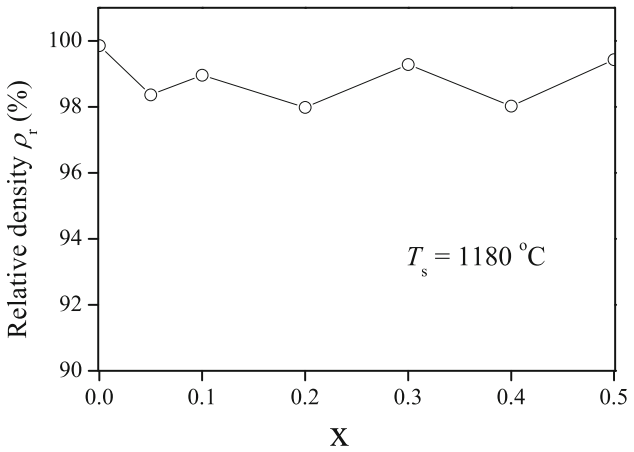

Fig. 4. The relative density ρ_r for the CBT-Eu-*x* ceramics.

continuous scanning type in the 2θ range of 20°–70°. The microstructures of the ceramics were observed by scanning electron microscopy (SEM, FEI-Quanta 250; FEI, Portland, OR, USA). The bulk density ρ of the sintered ceramics was measured by the Archimedes' method with deionized water (ρ_{H_2O} = 0.997 g/cm^3, 25°C) as the liquid media. The average grain size D_A was obtained by multiplying the average linear intercept length of grains by 1.56.[18] The photoluminescence (PL) and photoluminescence excitation (PLE) spectra were recorded using a spectrophotometer F-7000 (Hitachi High-Tech.) equipped with a 150-W xenon lamp as the excitation source. The polarization hysteresis (*P*–*E*) loops were measured at 200°C in a silicone oil bath using a precision ferroelectrics measuring system (Premier II; Radiant Technologies, Northford, CT, USA). The planar electromechanical coupling factor k_p was determined by the resonance method according to the IEEE Standards 176 using an impedance analyzer (Agilent 4294A; Agilent Technologies). The piezoelectric constant d_{33} was measured using a piezo-d_{33} meter (ZJ-3A; Institute of Acoustics, Chinese Academy of Science, Beijing, China).

RESULTS AND DISCUSSION

Figure 1 shows the XRD patterns of the CBT-Eu-*x* ceramics. The diffraction peaks of the samples can be indexed according to an orthorhombic space group $A2_1am$. From Fig. 1a, it was found that all the samples have a pure Aurivillius-type structure, and no secondary phase was detected, indicating that Eu^{3+} ions have been successfully incorporated into the CBT lattice to form a solid solution. Moreover, the highest intensity of the (119) diffraction peak was observed in all ceramics, which is consistent with the fact that the most intense reflection of BLSFs is from the (112 m + 1) planes.[3] From Fig. 1b, it can be noted that the diffraction peaks shift slightly to higher 2θ angles on the *x* increase 0–0.5, which should be ascribed to the partial substitution of Bi^{3+} ($r_{Bi^{3+}}$ = 1.03 Å, CN = 6) by smaller Eu^{3+} ($r_{Eu^{3+}}$ = 0.947 Å, CN = 6) ions. This is consistent with a previous report.[19] As for the BLSFs compounds, it has been confirmed that the bismuth oxide layer is very stable, and that the Bi^{3+} cations in $(Bi_2O_2)^{2+}$ are difficult to be substituted in a lower concentration of other rare earth ions.[15] Osada et al.[20] also reported that La^{3+} cannot substitute the Bi^{3+} in the $(Bi_2O_2)^{2+}$ layer in $Bi_4Ti_3O_{12}$ when the La

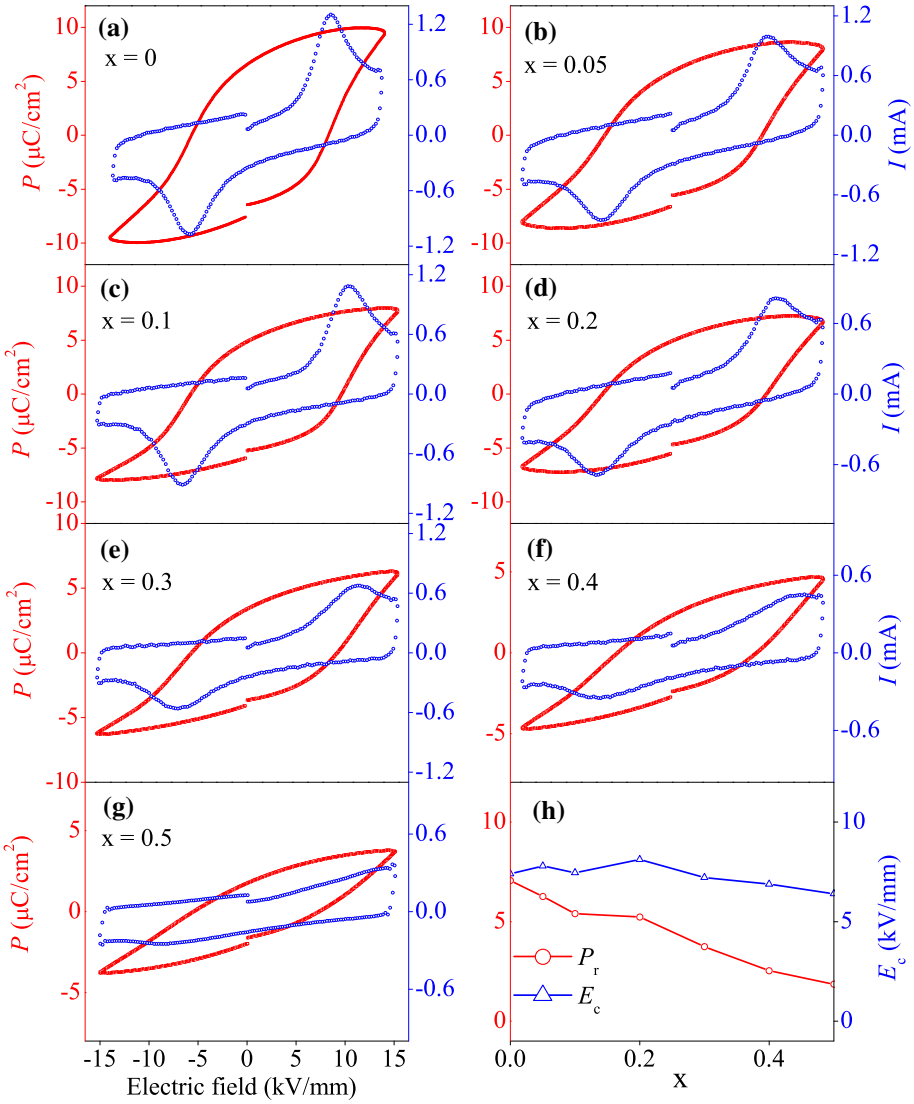

Fig. 5. (a–g) *P–E* (red line) and *I–E* (blue line) loops of the CBT-Eu-*x* ceramics measured under an electric field of 15 kV/mm at 200°C temperature; (h) composition dependence of the remanent polarization P_r and coercive filled E_c for the CBT-Eu-*x* ceramics.

content is lower than 1.0. Therefore, Eu^{3+} ions in CBT-Eu-*x* ($x \leq 0.5$) ceramics may enter A sites of the pseudo-perovskite block to form a solid solution.

In order to characterize the variation of the orthorhombic structure, a general diffraction/reflectivity analysis program, MAUD,[21] was used to perform a full-pattern matching using the Rietweld method and to refine the lattice parameters of the ceramics. Based on the XRD patterns of CBT-Eu-*X* ceramics shown in Fig. 1, the lattice parameters *a*, *b* and *c* of the ceramics were defined, as shown in Fig. 2. The observed parameter *a* decreases gradually from 5.4301 Å to 5.4180 Å with *x* increasing from 0 to 0.5, and the observed *b* and *c* values increase firstly from 5.4096/40.6973 Å to 5.4146/40.7294 Å with *x* increasing from 0 to 0.2 and then decrease slightly to 5.4092/40.7144 Å with *x* further increasing to 0.5. The variation of lattice parameters should be attributed to the distortion of the orthorhombic structure caused by the substitution of smaller Eu^{3+} for Bi^{3+}. The composition dependences of orthorhombicity of the CBT-Eu-*x* ceramics are shown in the inset of Fig. 2. The orthorhombicity is defined as $2(a - b)/(a + b)$.[22] It can be observed that the value of orthorhombicity decreases gradually from 3.78×10^{-3} to 7.77×10^{-4} with *x* increasing from 0 to 0.5, suggesting that the distortion of the orthorhombic structure appears and becomes weakened gradually, which may have an important effect on microstructure, ferroelectric properties of the materials.

Figure 3 shows the SEM images of the as-sintered surface microstructure of CBT-Eu-*x* ceramics with *x* = 0, 0.05, 0.1, 0.2, 0.3, 0.4 and 0.5. From Fig. 3, typical plate-like grains with random orientation are observed and all the samples have a dense structure. Some researchers have reported that the {001} plane possesses a lower surface energy, which

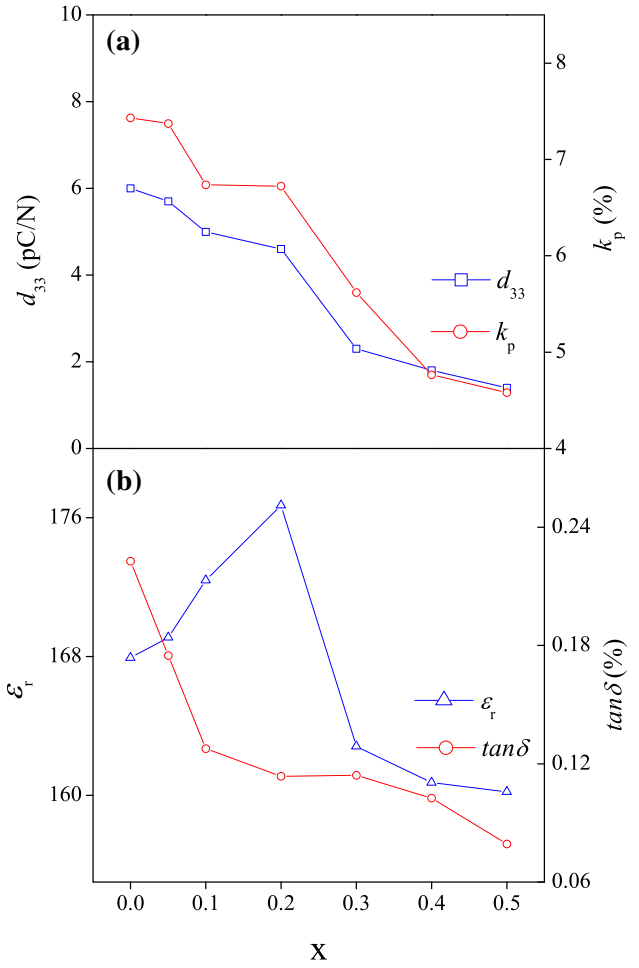

Fig. 6. Composition dependences of (a) piezoelectric constant d_{33}, electromechanical coupling factor k_p, (b) dielectric constant ε_r and loss factor tanδ for CBT-Eu-x ceramics.

suggests that the grain growth rate along the $a - b$ plane is faster than that along the c-axis and thus a plate-like morphology is observed.[23] The average grain size decreases gradually from 2.19 μm to 1.61 μm with x increasing from 0 to 0.5, indicating that Eu^{3+} doping suppresses the grain growth of CBT ceramics, which is attributed to the larger bond energy of the Eu-O band than that of the Bi-O band. This phenomenon has been reported previously.[24,25] The relative density ρ_r of the CBT-Eu-x ceramics is shown in Fig. 4. For all the CBT-Eu-x ceramics, the relative density shows a weak dependence on x and gives high ρ_r values of 97.9–99.7%.

Figure 5a–g shows the P-E and I–E loops of the CBT-Eu-x ceramics measured under an electric field of 15 kV/mm at 200°C, while Fig. 5h shows the composition dependence of the P_r and E_c in the CBT-Eu-x ceramics. From Fig. 5a–g, it can be seen that typical and saturated P–E loops are obtained for all the ceramics. From Fig. 5h, the observed remanent polarization P_r decreases gradually from 7.07 to 1.86 μC/cm^2 with x increasing from 0 to 0.5, while the observed coercive field E_c presents a weak dependence on x and remains in the range of 6.40–7.79 kV/mm at $x = 0 - 0.5$. The ferroelectric domain switching demonstrated by current peaks in the I–E curves are observed with x increasing from 0 to 0.3. However, the I–E loops have no apparent polarization switching behavior for the ceramics with $x = 0.4$ and 0.5. It is well known that ferroelectric properties could be related to the distortion of the orthorhombic structure.[8,25] It has been proved that the value of the orthorombicity decreases with increasing x. Therefore, the ferroelectric properties

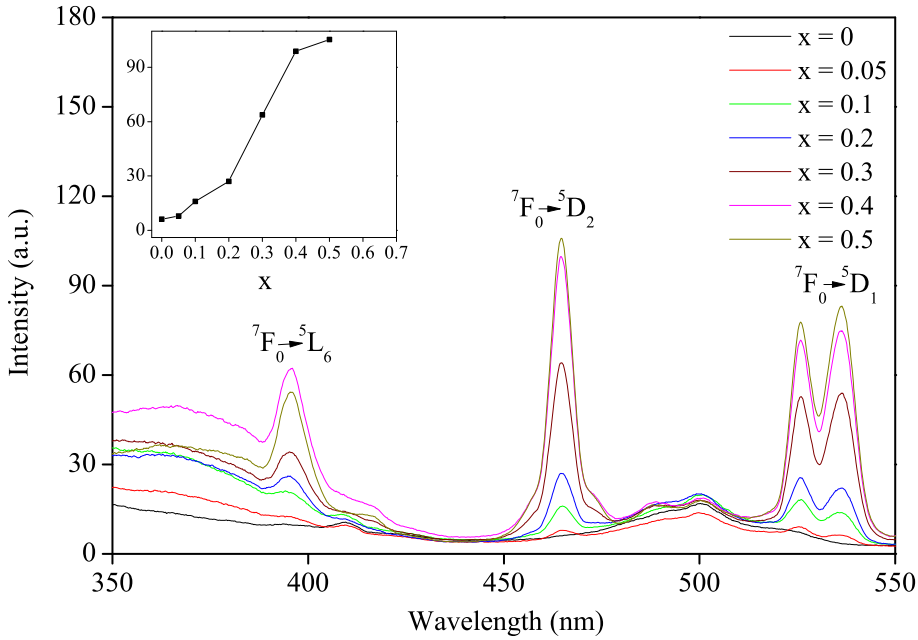

Fig. 7. Excitation spectra of the CBT-Eu-x ceramics monitored at 616 nm.

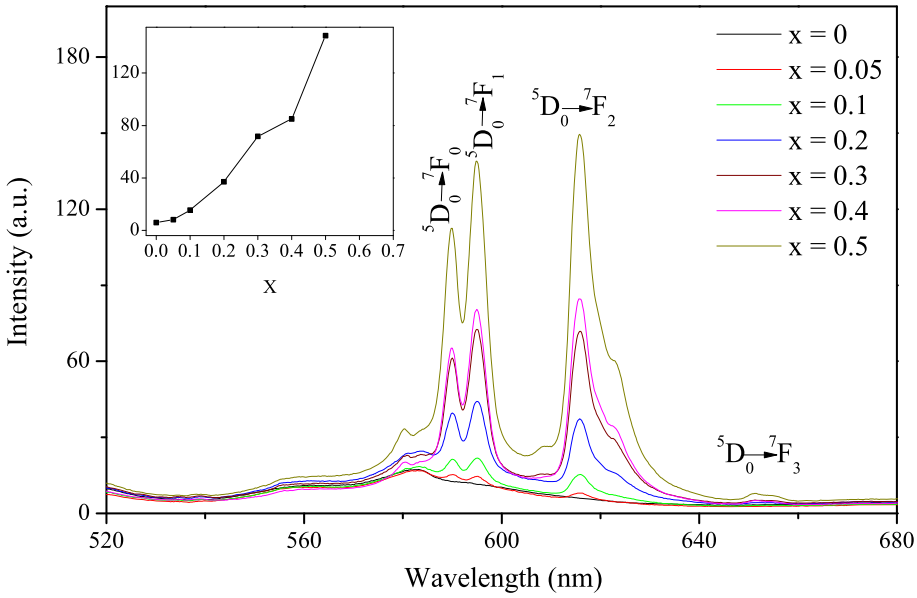

Fig. 8. Emission spectra of the CBT-Eu-x ceramics excited at 465 nm.

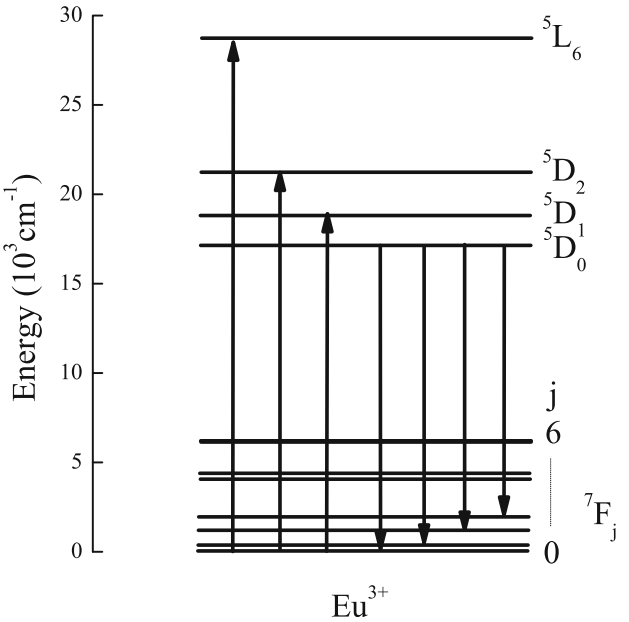

Fig. 9. Energy level scheme of Eu^{3+}.

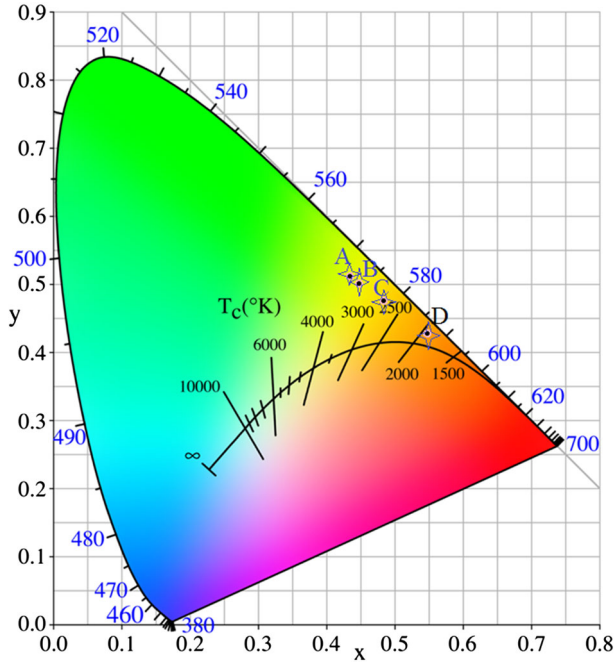

Fig. 10. CIE chromaticity coordinates of the CBT-Eu-x (x = 0.05, 0.1, 0.3, 0.5) ceramics with the emission which excited 465 nm.

deteriorated in the ceramics at high Eu doping levels.

The composition dependences of d_{33}, k_p, ε_r and tanδ of CBT-Eu-x ceramics are shown in Fig. 6. In Fig. 6a, the observed d_{33} decreases monotonously from 6.0 pC/N to 1.4 pC/N with x increasing from 0 to 0.5. Similarly, the observed k_p decreases monotonously from 7.4% to 4.6%. In Fig. 6b, the observed ε_r increases with x increasing from 0 to 0.2 and then decreases with x further increasing to 0.5, giving a maximum value of 177 at x = 0.2. The observed tanδ decreases gradually with increasing x. Obviously, Eu doping degrades the piezoelectricity of the ceramics.

Figure 7 shows the excitation spectra of the CBT-Eu-x ceramics monitored at 616 nm. Several sharp peaks can be seen at 396 nm, 465 nm and 536 nm, which are ascribed to the typical f–f transitions of Eu^{3+} from the $^7F_0$ ground state to the $^5L_6$, $^5D_2$ and $^5D_1$ excited states of Eu^{3+}, respectively. The inset in Fig. 7 reveals the dependence of the excitation intensity on the Eu^{3+} concentration. It can be

observed that the excitation intensity increases significantly with x increasing from 0 to 0.5.

Figure 8 displays the emission spectra of the CBT-Eu-x ceramics excited at 465 nm. Under the resonant excitation wavelength of 465 nm, several narrow spectral lines are obtained. Three main emission bands located at 590 nm, 595 nm and 616 nm are assigned to the transitions of the $^5D_0$–$^7F_0$, $^5D_0$–$^7F_1$, and $^5D_0$–$^7F_2$ levels of Eu^{3+}, respectively. The emission peak near 616 nm should be attributed to the electric dipole transition, suggesting that Eu^{3+} occupies a non-centrosymmetric site in $CaBi_4Ti_4O_{15}$ host lattices,[26] which is consistent with the distortion of the lattice (Fig. 1). Furthermore, it can be noted that the emission peak position shows almost no significant changes, while the strong change of the peak shape is evident because of great peak magnitude variation. Compared with some Eu^{3+}-containing oxides [e.g., $YNbO_4$:Eu^{3+}, $CsGd_{1-x}Eu_x(MoO_4)$ and α-$Eu_2(MoO_4)_3$],[27–29] the emission peak shape is different for our materials. We found that the ^7F_J energy levels of Eu^{3+} ions split into several components, which may be ascribed to the crystal-field effect.[30] In addition, for our materials, the largest R is about 1.4, which is defined as the intensity ratio of ($^5D_0$–$^7F_2$) to ($^5D_0$–$^7F_1$). The value is smaller than that of the above materials, indicating the lower asymmetric ratio. The inset in Fig. 8 presents the dependence of the emission intensity on the Eu^{3+} concentration. It can be seen that the emission intensity increases greatly with increasing x.

In order to illustrate clearly the photoluminescence process, the simplified energy level diagram is plotted in Fig. 9. According to the energy level diagram for Eu^{3+} and selection rules, the electrons with $^7F_0$ ground state are excited to the $^5D_2$ high level under the 465 nm light excitation, and the $^5D_2$ level are radiationlessly relaxing to the $^5D_0$ state and then subsequently recombining to the lower level of ^7F_j (j = 0, 1, 2, 3). As a result, a strong red emission is observed, as shown in Figs. 7 and 8. The weak red emission centered at 655 nm corresponds to the $^5D_0$–$^7F_3$ transition.

Figure 10 shows the CIE chromaticity coordinates of the CBT-Eu-x ceramics with the emission spectra excited at 465 nm. According to the CIE standards, the chromaticity coordinates based on the emission spectrum of the CBT-Eu-x ceramics were calculated. From Fig. 10, the CIE coordinates (x, y) vary systematically from x = 0.05 (0.4344, 0.5124) (A), x = 0.1 (0.4484, 0.5009) (B), x = 0.3 (0.4841, 0.4755) (C) to x = 0.5 (0.5478, 0.4282) (D) as the Eu^{3+} concentration increases. It can also be observed that the emission color shifts slightly to the longer wavelength region with increasing x. This phenomenon can be ascribed to the variation of the rystal-field environment of Eu^{3+} ions. The above results reveal that the Eu-doped CBT ceramics are a potential phosphor for LED under blue excitations.

CONCLUSIONS

Eu-doped $CaBi_4Ti_4O_{15}$ ceramics were successfully fabricated by a traditional solid state method, and the effects of Eu doping on the structure, ferroelectric, piezoelectric and photoluminescence properties of the ceramics were investigated. A typical bismuth oxide-layered structure and plate-like grain were examined by XRD and SEM, respectively. The remanent polarization P_r and the piezoelectric coefficient d_{33} decreased with the increasing Eu content. The photoluminescence excitation spectra showed the sharp excitation peak centered at 465 nm due to the f–f transition from the $^7F_0$ ground state to the $^5D_2$ excited state of Eu^{3+}. Under the excitation by 465 nm light, the sample exhibited emission peak centered at 616 nm corresponding to the $^5D_0$–$^7F_2$ transition in Eu^{3+}. Our results suggest that Eu-doped CBT is a promising multifunctional material.

ACKNOWLEDGEMENT

This work was supported by the projects of Education Department of Sichuan Province (11ZA104), Science and Technology Bureau of Sichuan Province (2010JQ0046) and the Open Project of State Key Laboratory of Electronic Thin Films and Integrated Devices of University of Electronic Science and Technology of China (KFJJ201108).

REFERENCES

1. P. Yang, S. Peng, and X.B. Wu, et al., *J. Phys. D Appl. Phys.* 42, 015005 (2009).
2. N. Yasuda, T. Banno, and K. Fujita, et al., *J. Phys.: Condens. Matter* 18, 7659 (2006).
3. C.M. Wang, J.F. Wang, and L.M. Zheng, et al., *Mater. Sci. Eng. B* 171, 79 (2010).
4. Z.H. Peng, F.K. Huang, and Q. Chen, et al., *Ferroelectrics* 447, 69 (2013).
5. G.R. Li, L.Y. Zheng, and Q.R. Yin, et al., *J. Appl. Phys.* 98, 064108 (2005).
6. J.T. Zeng, Y.X. Li, and D. Wang, et al., *Solid State Commun.* 133, 553 (2005).
7. X.H. He, B. Wang, and X.Y. Fu, et al., *J. Mater. Sci: Mater. Electron.* (2014). doi:10.1007/s10854-014-2031-y.
8. W. Wang, H.W. Zheng, and Y.F. Liu, et al., *J. Phys. D Appl. Phys.* 42, 105411 (2009).
9. D.F. Peng, X.S. Wang, and C.N. Xu, et al., *J. Am. Ceram. Soc.* 96, 184 (2013).
10. D.F. Peng, H.Q. Sun, and X.S. Wang, et al., *Mater. Sci. Eng. B* 176, 1513 (2011).
11. S. Fuentes, N. Barraza, and E. Veloso, et al., *J. Alloys Compd.* 569, 52 (2013).
12. V. Sharma, A. Das, and V. Kumar, et al., *J. Mater. Sci.* 49, 2225 (2014).
13. Z.P. Yang, P.F. Liu, and J.J. Li, et al., *J. Alloys Compd.* 578, 118 (2013).
14. Y.M. Jia, Z.H. Zhou, and Y.B. Wei, et al., *J. Appl. Phys.* 114, 213903 (2013).
15. D.F. Peng, H. Zou, and C.N. Xu, et al., *Ferroelectrics* 450, 113 (2013).
16. T. Wei, Q.J. Zhou, and C.Z. Zhao, et al., *Ceram. Int.* 39, 7211 (2013).
17. A. Tarafder, A.R. Molla, and S. Mukhopadhyay, et al., *J. Am. Ceram. Soc.* 95, 1851 (2012).
18. X.H. Wang, P.L. Chen, and I.W. Chen, et al., *J. Am. Ceram. Soc.* 89, 431 (2006).

19. N. Thongmee, A. Watcharapasorn, and S. Jiansirisomboon, et al., *Ferroelectrics* 458, 76 (2014).
20. M. Osada, M. Tada, and M. Kakihana, et al., *Jpn. J. Appl. Phys. Part 1* 40, 5572 (2001).
21. L. Lutterotti, *MAUD*, *Material Analysis Using Diffraction*. (2011). http://www.ing.unitn.it/maud/index.html.
22. S.S. Kundu, D.A. Ochoa, and J.E. Garcia, et al., *Mater. Chem. Phys.* 136, 680 (2012).
23. G. Parida and J. Bera, *Phase Transitions* 87, 452 (2014).
24. X.J. Chou, J.W. Zhai, and H.T. Jiang, et al., *J. Appl. Phys.* 102, 084106 (2007).
25. H.W. Zheng, X.Y. Liu, and W.C. Wang, et al., *J. Sol–Gel. Sci. Technol.* 58, 539 (2011).
26. A.R. Molla, A. Tarafder, and S. Mukherjee, et al., *J. Am. Ceram. Soc.* 96, 2387 (2013).
27. Lj.R. Đačanin, M.D. Dramićanin, and S.R. Lukić-Petrović, et al., *Ceram. Int.* 40, 8281 (2014).
28. P.L. Shi, Z.G. Xia, and M.S. Molokeev, et al., *Dalton Trans.* 43, 9669 (2014).
29. V.V. Atuchin, A.S. Aleksandrovsky, and O.D. Chimitova, et al., *J. Phys. Chem. C* 118, 15404 (2014).
30. G.S.R. Raju, E. Pavitra, and G. Nagaraju, et al., *Dalton Trans.* 40, 1790 (2015).